

## Cyclic true stress true strain relation in the large strain region of common steel for welded structures

Matsuda, Kazuki

Department of Marine Systems Engineering, Faculty of Engineering, Kyushu University

Shimoka, Tsukasa

Department of Naval Architecture and Ocean Engineering, Graduate School of Engineering, Kyushu University

Murakami, Koji

Technical Division, School of Engineering, Kyushu University

Uchimura, Tomoya

Technical Division, School of Engineering, Kyushu University

他

<https://hdl.handle.net/2324/7159364>

---

出版情報 : Welding International. 38 (3), pp.239-248, 2023-11-10. Taylor & Francis Group  
バージョン :  
権利関係 :



## Cyclic true stress true strain relation in the large strain region of common steel for welded structures\*

by MATSUDA Kazuki\*\*, SHIMOKA Tsukasa\*\*\*, MURAKAMI Koji\*\*\*\*,  
UCHIMURA Tomoya\*\*\*\* and GOTOH Koji\*\*

Cyclic true stress - true strain curves were obtained using general-purpose shipbuilding steel in the large strain region. Test methods are incremental step test and static tensile test after cyclic loading. The stress-strain curves for static and cyclic loading were compared to investigate the cause of the difference between each other. A simple method for estimating the cyclic stress-strain curves was proposed. The diameter and curvature of the smallest cross-section of the specimen were measured using telecentric measurement device, and the true stress - true strain curve was obtained using the Bridgman correction method. Using the measurement method, cyclic stress-strain diagrams were obtained in the region where the true strain exceeded 1% by performing cyclic tensile tests using the incremental step method and static tensile tests after cyclic loading. The influence of the test method and maximum displacement conditions on the cyclic stress-strain curve was small within the scope of this study. There was little difference in the elongation between the static tensile test and the static tensile test after cyclic loading. The difference in yield stress between static and cyclic loading was discussed in terms of macro-yield mechanisms at intergranular and transgranular. A simple method for estimating cyclic stress-strain curves from a static stress-strain curve was proposed. The specimens used in this study are general-purpose shipbuilding steels, and the results should be applicable to similar steels for welding and structures.

**Key Words:** Cyclic stress strain curve, Incremental step method, Static tensile test after cyclic loading, Yield stress, Common steel for welded structures, Ship Building steel, Telecentric measurement

### 1. Background

Cyclic deformation or cyclic stress loading on a material causes fatigue cracking, which eventually leads to rupture. Fatigue cracking is known to be more difficult to prevent than ductile or brittle fracture because it is caused by stress loading below the yield point of the material. As part of the complexity of fatigue phenomena, it is known that the stress-strain diagram changes under cyclic tension compared to static tension. Toyosada et al.<sup>1)</sup> proposed a fatigue crack propagation law with the parameter of re-tensile plastic zone generated (RPG) loading at the fatigue crack tip. The authors further developed fatigue cracking simulations in which the dimensions of the alternating-plastic region, which is the region where the tensile and compressive plastic deformation regions at the crack tip overlap, were used as parameters.<sup>2)</sup> These simulations require the input of the stress-strain relationship of the material of interest. For simplicity, it is more convenient to use the yield point obtained in a static tensile test. However, since fatigue crack propagation is a phenomenon that occurs under cyclic loading, the stress-strain relationship should be based on data obtained under cyclic loading. However, obtaining cyclic stress-strain diagrams requires a higher test cost than that of static loading stress-strain diagrams<sup>3)</sup>. In general, cyclic stress-strain diagrams can be obtained by applying cyclic loads of constant amplitude to multiple specimens and smoothly connecting the apexes of the loops at each amplitude when the hysteresis loops become stable and steady-state. Ma et al.<sup>4)</sup> proposed a method that can estimate cyclic stress-strain diagrams from static tensile tests and two levels of cyclic loading tests. However, the test cost is still high, given that the stress-strain diagram for static loading is obtained from only one specimen. Landgraf et al.<sup>5)</sup> proposed a method called the incremental step method, which can obtain cyclic stress-strain diagrams on a single specimen. This test procedure is described below, but the test cost to obtain cyclic stress-strain diagrams can be significantly reduced by this method. Because of the difficulty of measurement, few cyclic true stress true strain diagrams have been reported in the large-strain region, but recent advances in measurement equipment have made measurement relatively easy. Many attempts to obtain cyclic stress-strain diagrams by estimation without measurement have been reported in the past. Lopez et al.<sup>6)</sup> summarized the stress-strain relationships of various steels under static and cyclic loading and proposed an estimation equation for cyclic stress-strain characteristics using tensile strength and Brinell hardness. Zhang et al.<sup>7)</sup> proposed an estimation equation using yield stress, tensile strength, and elongation at break.

\*Date of receipt: February 22, 2023 / Date of acceptance: June 26, 2023

\*\* Member, Department of Marine Systems Engineering, Faculty of Engineering, Kyushu University

\*\*\* Department of Naval Architecture and Ocean Engineering, Graduate School of Engineering, Kyushu University

\*\*\*\* Technical Division, School of Engineering, Kyushu University

Many other methods for estimating cyclic stress-strain relationships<sup>8-11)</sup> have been proposed, but most of them are not accompanied by a consideration from a materials engineering standpoint.

In this study, we report the results of obtaining cyclic true stress-true strain diagrams in the large-strain region using general welding steel as the specimen. The causes of the differences between static and cyclic loading are discussed by comparing the stress-strain diagrams, and a simple method for estimating cyclic stress-strain diagrams based on a materials engineering viewpoint is also presented.

## 2. Experiment

The specimen was KD36 steel (NK), which is widely used as a general-purpose shipbuilding steel, with a plate thickness of 17 mm. Table 1 shows the mechanical properties of the specimens. Hourglass-shaped round bar specimens with a minimum cross-sectional diameter of 10 mm were taken from the specimens as shown in Fig. 1.

### 2.1 Tensile test conditions

In this study, the specimens shown in Fig. 1 were subjected to cyclic tensile and compression tests using the incremental step method proposed by Landgraf et al. and to static tensile tests after being subjected to cyclic loading using the incremental step method for a specified number of times. The former is referred to as a cyclic tensile and compression test and the latter as a static tensile test after cyclic loading. Static tensile tests were also conducted at a crosshead displacement rate of 0.2 mm/min to compare stress-strain diagrams. A 50 kN servohydraulic fatigue testing machine manufactured by Shimadzu Corporation was used for all tensile tests. In the static tensile test, a strain gauge with a gauge length of 6 mm was affixed to the smallest cross-sectional section to measure the axial strain during the test.

An example of the loading waveform of one block in the incremental step method is shown in Fig. 2. In this method, a hysteresis loop (relationship between stress and strain) is obtained by applying a load waveform in which the maximum and minimum values of the load gradually increase and decrease, as shown in Fig. 2. Then, by connecting the vertices of each loop, a cyclic stress-strain diagram can be obtained from a single specimen. The test conditions were based on those of Nishikawa et al.<sup>12)</sup>, where the mean stress was set to 0 (stress ratio  $R = -1$ ) in displacement control, the maximum displacement was set for each condition, and the maximum and minimum displacements were set for each cycle in a linear fashion so that the maximum displacement was at the center of the block during 25 cycles per block. The crosshead displacement rate was kept constant, and the displacement rate for each test was the maximum displacement [mm]  $\times 0.0385$  [1/s]. For example, under the maximum displacement condition of 1.3 mm, the displacement velocity is 0.05 mm/s. Table 2 shows the maximum displacement for each condition in the cyclic tensile and compression tests. The test was conducted until the specimen ruptured.

**Table 1** Mechanical properties of material used.

Yield Stress	Tensile Strength	Elongation	Young's modulus
[MPa]	[MPa]	[%]	[GPa]
403	515	24	206

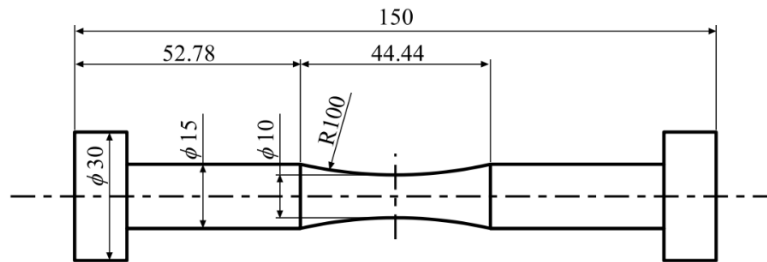


**Fig. 1** Geometry of the specimen.

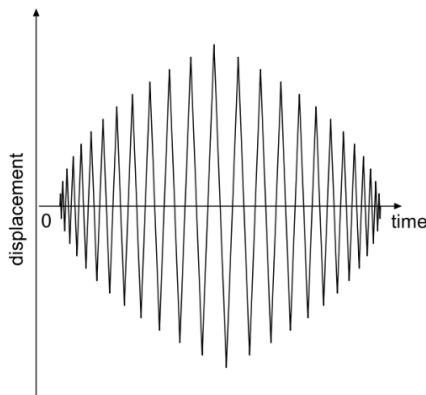


**Fig. 2** Schematics of a block shape of incremental step.

**Table 2** Lists of maximum displacement conditions.

Maximum Displacement
[mm]
$\pm 0.75$
$\pm 0.85$
$\pm 0.95$
$\pm 1.0$
$\pm 1.3$

The conditions for the static tensile test after cyclic loading by the incremental step method were as follows: After cyclic loading of half the number of loaded blocks up to rupture at each maximum displacement shown in Table 2 (plus 3/4 and 1/4 of the number of ruptured blocks for the  $\pm 0.75$  mm maximum displacement condition), a static tensile test was conducted at a crosshead displacement rate of 0.2 mm/min.

## 2.2 Calculation of True Stress and True Strain

True strain and true stress during tensile testing were determined by measuring the diameter and curvature of the smallest cross-sectional section of the specimen using a Keyence TM-X5040 telecentric measurement device, and were derived using the correction method<sup>13)</sup> by Bridgman as follows.

$$\varepsilon_t = 2 \cdot \ln \left( \frac{r_0}{r} \right) \quad (1)$$

$$\sigma_t = \frac{P}{\pi r^2 \left( 1 + 2 \frac{R}{r} \right) \log \left( 1 + \frac{1}{2} \frac{r}{R} \right)} \quad (2)$$

where,  $R$ : radius of curvature of the neck [mm]  
 $r$ : radius of cross section at minimum cross section [mm]  
 $r_0$ : Initial cross-section radius at minimum cross-section [mm]  
 $P$ : Test load [N]

It has been reported that this method has a problem with correction accuracy during large deformation<sup>14)</sup>, and Murata et al.<sup>15)</sup> found that the Bridgman correction overestimates stress values compared to actual behavior during large deformation. However, the Bridgman correction was used in this study, keeping in mind the results of these previous studies, because the correction methods that are considered to be more accurate are often not easy to apply and have not been verified on a wide range of materials. For comparison with this derivation method, strain gauges were affixed to the smallest cross section in the static tensile test and strain was measured as described above.

## 2.3 Cross-sectional observation

Cross-sectional observation samples were taken near the 1/4 position of the plate thickness of the specimens that had not been subjected to specimen fabrication, subjected to nital etching, and the microstructure was observed using an optical microscope.

## 3. Results

### 3.1 Static tensile test

The true stress to true strain diagram obtained from the static tensile test is shown in Fig. 3. Note that, the graphs (a) through (c) are identical except for the values of the vertical (true stress) and horizontal (true strain) axes. Fig. 3 plots the stress/strain relationships obtained by the strain gauge and the projection image analyzer, respectively. (b) shows that the stress-strain diagrams obtained from strain gauge and projected image measurements are in close agreement when the flow stresses after yielding are compared. In the range where the true strain exceeds approximately 0.02, strain gauges have not been able to measure the strain. This was due to the gauge detaching from the specimen. Since the strain measurement limit is 0.05 according to the gauge specifications, it is considered that the gauge was detached somewhat early in this test due to a defect in the attachment.

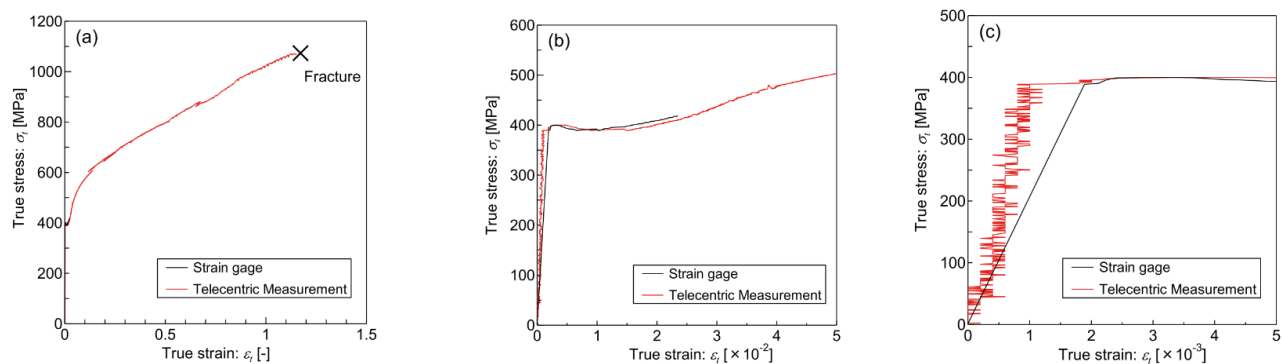


**Fig.3** True stress-true strain curves obtained in monotonic static tensile test. (a) true strain to 1.5, (b) to 0.05, (c) to 0.005

**Table 3** Lists of number of loading blocks to failure for each condition.

Maximum Displacement [mm]	Number of loading blocks to failure [blocks]
$\pm 0.75$	37
$\pm 0.85$	22
$\pm 0.95$	13
$\pm 1.0$	12
$\pm 1.3$	6

Meanwhile, (c) shows that in the range of true strain less than 0.002, which is considered to be the elastic range, the variation of the plots obtained by projection image measurement is large. This may be partly due to the fact that strain changes little with increasing stress in the elastic region, and partly because strain was derived under the assumption of constant volume. The true stress-strain relationship measured and derived by the projection image analyzer was found to be as accurate as the conventional strain gage measurement method in the elasto-plastic range, and was also able to measure large strains that cannot be measured by strain gauges.

### 3.2 Cyclic tensile and compression test

Table 3 lists the number of load blocks loaded to failure for each maximum displacement condition in cyclic tensile and compression tests using the incremental step method. The true stress-true strain relationship (hysteresis loop) obtained at half the number of blocks to failure shown in Table 3 and the cyclic stress-strain diagram obtained by connecting the maxima and minima at each hysteresis are shown in Fig. 4. Note that buckling was observed at maximum displacements of  $\pm 1.0$  mm and  $\pm 1.3$  mm when compressive loads were applied, and was therefore excluded from the results. A comparison of the obtained cyclic stress-strain diagrams is discussed below.

### 3.3 Static tensile test after cyclic loading

The true stress true strain diagram obtained from the static tensile test after cyclic loading by the incremental step method is shown in Fig. 5. Note that the stress-strain diagrams for static loading are also plotted in Fig. 5 for comparison. (a) is a comparison of different maximum displacements with half the number of loaded blocks in both cases, and (b) is a comparison of maximum displacements of  $\pm 0.75$  mm in both cases and the number of loaded blocks at 1/4, half, and 3/4 of the way to failure. Comparison of the stress-strain diagram for the fracture strain with that for the static loading shows that the fracture strain hardly decreases even after cyclic loading.

### 3.4 Microstructural observation

A photograph of the microstructure of a nital-etched cross-sectional sample is shown in Fig. 6. Fig. 6 shows that the specimen has a mixed structure of ferrite and pearlite. From the cutting method (JIS G 0551: 2020), the average grain size of ferrite was  $9.60\text{ }\mu\text{m}$  with a standard deviation of  $2.29\text{ }\mu\text{m}$ .

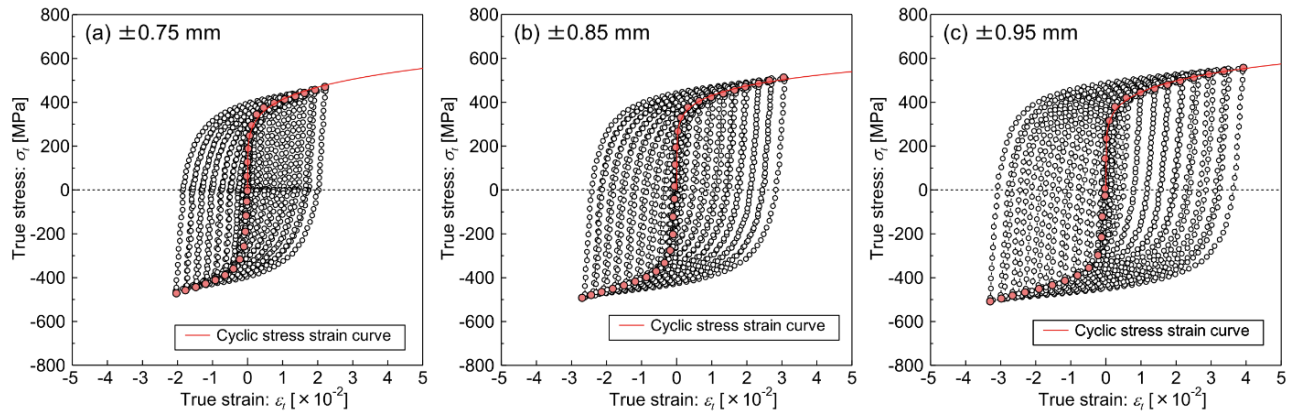


**Fig.4** Hysteresis loops and cyclic true stress-true strain curves obtained by incremental step test.

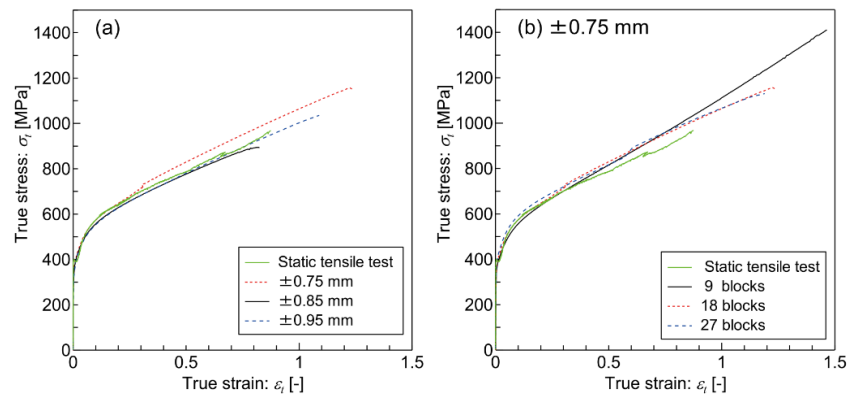


**Fig.5** True stress-true strain curves obtained from static tensile tests after cyclic tensile loading. (a) Difference in maximum displacement, (b) Difference in number of loading blocks.

#### 4. Discussion

The differences in the true stress true strain diagrams obtained from each test are compared. Next, a method for estimating cyclic stress-strain diagrams from stress-strain diagrams obtained from static tensile tests is discussed.

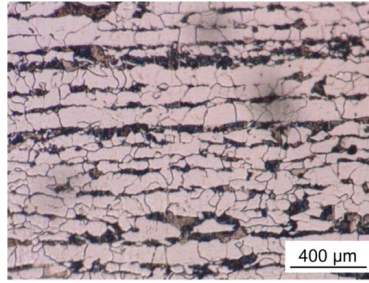


Fig.6 Microstructure of the specimen observed by optical microscopy.

##### 4.1 Comparison of stress-strain diagrams

A comparison of cyclic true stress true strain diagrams for different conditions of maximum displacement obtained in cyclic tensile and compression tests is shown in Fig. 7. Fig. 7 shows that the difference in maximum displacement has little effect on the cyclic stress-strain diagram. A comparison of the results of the cyclic post-loading static tensile test is then shown in Fig. 5, which indicates that the maximum displacement and the number of loading blocks have little effect on the stress-strain diagram. Polák et al.<sup>16)</sup> reported similar results regarding the effect of the number of load blocks. A comparison of the stress-strain diagrams obtained from the cyclic tensile-compression test and the cyclic post-loading static tensile test is then shown in Fig. 8. Fig. 8 shows stress-strain diagrams obtained at maximum displacements of  $\pm 0.75$ ,  $\pm 0.85$ , and  $\pm 0.95$  mm. As shown in Fig. 8, the difference in stress-strain diagrams between the two test methods is small. The above results indicate that, within the scope of this study, the difference between the cyclic stress-strain diagrams obtained by the incremental step method and those obtained by static tensile loading after cyclic loading, and the effect of the maximum displacement condition on the stress-strain diagrams are small.

A comparison of stress-strain diagrams obtained from static tensile and cyclic tensile and compression tests is then shown in Fig. 9.

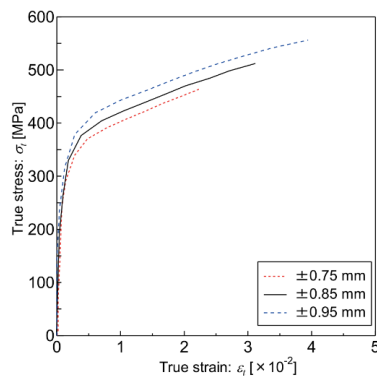


Fig.7 Comparison of cyclic stress-strain diagrams with different maximum displacements.

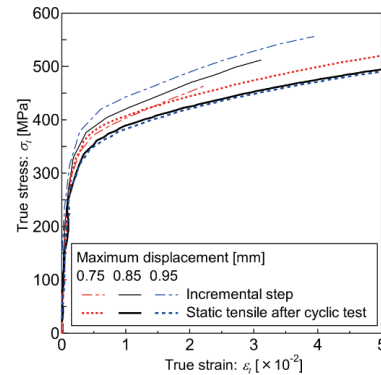


Fig.8 Comparison of cyclic stress-strain diagrams for different test methods.

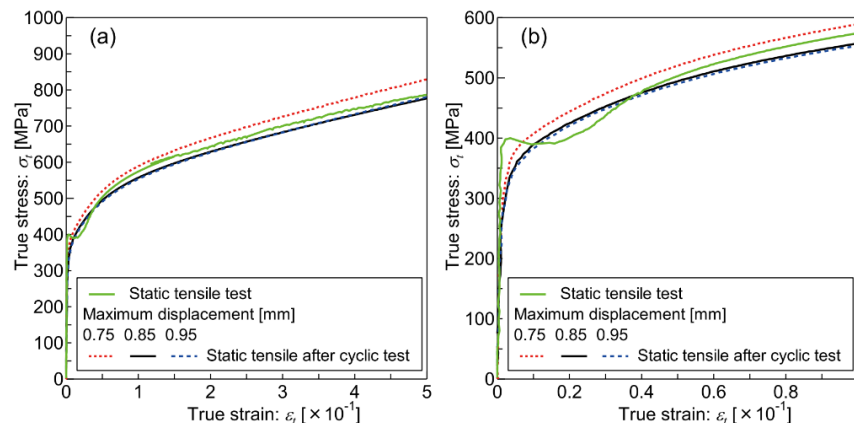


Fig.9 Comparison of stress-strain diagrams for static and cyclic loading. (a) True strain to 0.5, (b) True strain to 0.1

Fig. 9 shows that the stress-strain diagram from the static tensile test shows a linear increase in stress up to the yield stress and then a decrease in stress, while the stress-strain diagram from the cyclic tensile and compression tests shows a gradual curvature and transition to plastic deformation at lower stress values than the static tensile diagram. Then, in static tension, the stress is nearly constant in a region that appears to be the yield elongation. The stress then increases, which is in general agreement with the stress-strain diagram of the cyclic tensile and compression tests. It has been reported that the difference in stress-strain diagrams between static and cyclic loading, i.e., cyclic hardening and softening behavior, varies from material to material. For example, cyclic softening may occur in quenched and tempered steels<sup>17)</sup>, and the higher the tempering temperature, the greater the cyclic softening behavior<sup>5)</sup>. On the other hand, it has been reported that austenitic alloys such as SUS304 steel exhibit significant cyclic hardening behavior due to work-induced martensitic transformation<sup>18)</sup>. For the specimens in this study, the flow stress after yielding is not significantly different between static tensile loading and cyclic loading.

#### 4.2 Estimation of Cyclic Stress-Strain Diagrams

As mentioned in the background, obtaining cyclic stress-strain diagrams is more complicated than static stress-strain diagrams. Although there are methods to obtain cyclic stress-strain diagrams with a small number of specimens, such as the method used in this study, the hurdles to implementing these methods are still higher than those for static tensile testing, such as the need for testing equipment capable of cyclic loading. Therefore, a method for estimating cyclic stress-strain diagrams from static tensile test results would be highly useful.

One of the characteristics of cyclic loading is that the yield point is lower than that of static loading. It is understood that the high yield point obtained by static loading is partly due to the Cottrell atmosphere in which solid solution of C adheres to dislocations.<sup>19)</sup> However, in the present tests, no clear upper yield point was observed in static loading from Fig. 9 (b), and the stress was always lower in cyclic loading than in static loading in the range of true strains up to about 0.1, suggesting other causes for the lower yield point. By the way, it is known that yield stress decreases and yield elongation disappears, when temper rolling is applied during steel sheet production<sup>20)</sup>. Although this phenomenon is not cyclic loading, it has many similarities with the test results of this study, such as the fact that the yield point decreases to below the lower yield point under static loading due to processing. Takagi<sup>21)</sup> proposed two mechanisms that determine the macroscopic yielding of materials and explained this phenomenon. Yielding of polycrystalline materials is generally considered to be the result of dislocations deposited at grain boundaries causing stress concentrations that produce secondary dislocations and slip through the grain boundaries. Therefore, the Hall-Petch equation, which states that yield stress depends on grain size, is widely known, and the following relationship has been reported for low-carbon ferritic steels<sup>22)</sup>.

$$\sigma_{int} = \sigma_0 + 6 \times 10^{-4} / \sqrt{d} \quad (3)$$

where,  $\sigma_{int}$ : Yield stress based on intergranular dislocation [GPa]

$d$ : Grain size [m]

$\sigma_0$ : Frictional force (= 0.1) [GPa]

The friction force  $\sigma_0$  is a value that depends on alloy composition, temperature, and strain rate, etc. In the literature, a value of 0.1 GPa has been proposed, but the method used to determine it in this study is described later. This yielding, which is caused by dislocation release at grain boundaries, is called intergranular dislocation yielding. On the other hand, if the dislocations are bounded by solid solution elements, etc. within the grain, and the stress required to unbound the dislocations is higher than the stress that causes intergranular dislocation yielding, then the macroscopic yield stress is the stress that dislocations are unbound within the grain. This is called transgranular dislocation yielding. Thus, transgranular and intergranular dislocation yielding compete, with the higher yielding generally dominating the macroscopic yielding phenomena. According to Takagi, when an appropriate amount of movable dislocations exist in the base structure, such as after temper rolling, transgranular yielding occurs using these dislocations as a source, and macroscopic yielding occurs when the necessary stress is applied to them. Similarly, it is possible that the dislocations in the base microstructure may dominate the macroscopic transgranular dislocation yielding during cyclic loading. In other words, it is assumed that macroscopic yielding occurs during static tensile loading due to intergranular dislocation yielding, and macroscopic yielding occurs during cyclic loading due to transgranular dislocation yielding.

A method for estimating the yield stress at transgranular dislocation yielding is discussed. The effect of solid solution elements, etc. that affect transgranular dislocation yielding is considered to be included in the frictional force  $\sigma_0$  in equation (3). In addition, the following equation<sup>23)</sup> has been proposed as a formula for estimating the dislocation strengthening in grains  $\Delta \sigma$  [GPa].

$$\Delta \sigma \cong 1.8 \times 10^{-8} \sqrt{\rho} \quad (4)$$

where  $\rho$ : Dislocation density [ $\text{m}^{-2}$ ]

Tanaka et al.<sup>24)</sup> obtained the amount of dislocation to be introduced from the grain size and true strain  $\varepsilon_t$ . Equation (5) is a modified version of the relationship with the measured values.

$$\rho = 2.92 \times 10^{12} \sqrt{\varepsilon_t / d} \quad (5)$$

Substituting equation (5) into equation (4) and adding the frictional force of  $\sigma_0$  yields the yield stress  $\sigma_{trans}$  for transgranular dislocation yielding.

$$\sigma_{trans} = \sigma_0 + \Delta \sigma = \sigma_0 + 0.0307 \times \sqrt{\varepsilon_t / d} \quad (6)$$

Using the above equations, a simple method for estimating cyclic stress-strain diagrams is described. First, the yield stress  $\sigma_{int}$ , the true strain at that time  $\varepsilon_t$ , and the average grain size are obtained from static tensile tests and from observation of the specimen's microstructure. The friction force  $\sigma_0$  is then obtained from equation (3), and the cyclic yield stress  $\sigma_{trans}$  is estimated using equation (6). For simplicity, the hardening law of powers is used to estimate the stress-strain diagram. Substituting  $\sigma_{trans}/E$  as the strain corresponding to the yield stress  $\sigma_{trans}$ , taking into account the fact that the deformation is elastic until the cyclic yield stress  $\sigma_{trans}$ , the coefficient  $K$  of the power hardening law is obtained by the following equation.

$$K = \frac{E^n}{\sigma_{trans}^{n-1}} \quad (7)$$

where,  $E$ : Young's modulus [MPa],  $n$ : work hardening exponent



From Fig. 9, considering that the stress-strain diagrams for static and cyclic loading are almost identical except for the transient region from yield elongation immediately after yielding to uniform plastic elongation, the work hardening exponent is obtained from the stress-strain data after this transient region by the least-squares method, considering equation (7).

The cyclic stress-strain diagram estimated by the above method is shown in Fig. 10. For comparison, Fig. 10 shows the static loading stress-strain diagram, the cyclic stress-strain diagram at each maximum displacement, and the static loading stress-strain diagram after cyclic loading. Fig. 10 shows that the cyclic stress-strain diagram obtained by this method is in good agreement with the cyclic stress-strain diagram obtained in the test. The specimens used in this study are general-purpose shipbuilding steels, and the results should be applicable to similar welding or structural steels.

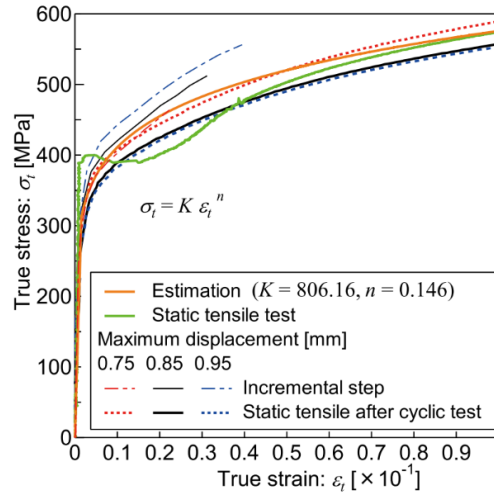


Fig.10 Comparison of stress-strain diagrams for static and cyclic loading.

For reference, the dependence of grain size and true strain on yield stress during static loading and cyclic loading calculated by Equations (3) and (6) is shown in Fig. 11. In (a) the true strain  $\varepsilon_t$  is 0.002 and in (b) the grain size  $d$  is  $9.6 \mu\text{m}$  based on the observations in Fig. 6. From (a), the ratio of cyclic stress to yield stress under static loading increases as grain size increases. This is because the yield stress depends on  $-1/2$  power of grain size in static loading according to equation (3) and  $-1/4$  power of grain size in cyclic loading according to equation (6), respectively, and the ratio of the two is positively correlated with the grain size. From (b), the true strain only affects the yield stress  $\sigma_{\text{trans}}$  during cyclic loading, so the change behavior in (b) is equal to that of  $\sigma_{\text{trans}}$ . Although the yield stress ratio increases as the true strain value increases, the yield stress under cyclic loading is less than that under static loading even when  $\varepsilon_t$  reaches 1%. All of these trends were obtained from mathematical equations, and verification by testing is an issue to be addressed in the future.

## 5. Conclusions

In this study, we attempted to obtain cyclic true stress true strain diagrams in the large strain region using a general-purpose shipbuilding steel. The stress-strain diagrams for static and cyclic loading were compared to investigate the causes of the difference between the two, and a simple method for estimating cyclic stress-strain diagrams was studied. The results obtained are described below.

- The diameter and curvature of the smallest section of the specimen were measured with an telecentric measurement device and a true stress true strain diagram was obtained using the Bridgman correction method.
- Using the above measurement method, cyclic tensile and compression tests using the incremental step method and static tensile tests after cyclic loading were conducted to obtain cyclic stress-strain diagrams in the region where the true strain exceeds 1%.
- Differences in maximum displacement in the incremental step method had little effect on the behavior of the cyclic stress-strain diagram.

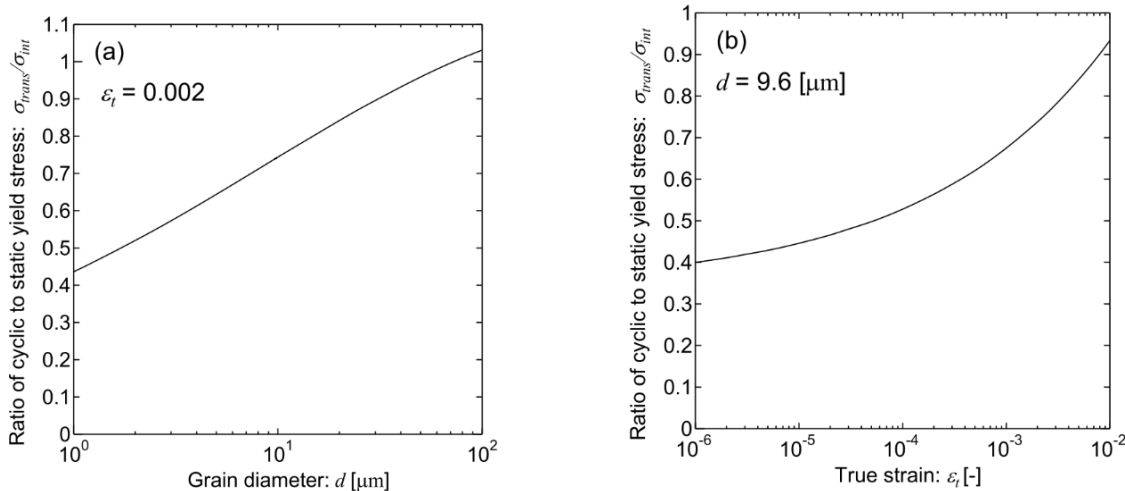


Fig.11 Dependence that ratio of cyclic to static yield stress by various parameter. (a) Grain diameter, (b) True strain



The differences in the stress-strain diagrams obtained from the incremental step method and the static tensile test after cyclic loading were small. The difference between the cyclic stress-strain diagrams obtained by the incremental step method and those obtained by static tensile loading after cyclic loading and the effect of the maximum displacement condition on the stress-strain diagrams were small in the range conducted in the present study. There was little difference in the fracture strain between the static tensile test and the static tensile test after cyclic loading.

● The difference in yield stress between static and cyclic loading is discussed from the viewpoint of macro-yield mechanisms at grain boundaries and within grains, and a simple method is proposed to estimate the stress-strain diagram under cyclic loading from the stress-strain relationship under static loading.

### Acknowledgment

This work was supported by JSPS Grant-in-Aid for Scientific Research JP20K21048.

### References

- 1) M Toyosada, K Gotoh, T Niwa: Fatigue crack propagation for a through thickness crack: a crack propagation law considering cyclic plasticity near the crack tip, *Int J Fatigue*, 26-9 (2004), 983-992.
- 2) K Yamaguchi, K Gotoh: Numerical Simulation of Fatigue Crack Propagation Considering the Alternating Plastic Behavior that Occurs Near the Crack Tip Using Elastic-Plastic Finite Element Analysis, *Conf Proc Jpn Soc Nav Archit Ocean Eng*, 32 (2021), 417-422. (in Japanese)
- 3) S Tsutsumi, K Murakami, K Gotoh, M Toyosada: Cyclic stress-strain relation under high cycle fatigue process -Elastoplastic constitutive model incorporating cyclic damage-, *Int J Nav Archit Ocean Eng*, 7 (2008), 243-250.
- 4) Z Ma, H Zhao, C Liu: Prediction Method of Low Cyclic Stress-Strain Curve of Structural Materials, *Mater Trans*, 56-7 (2015), 1067-1071.
- 5) R W Landgraf, J D Morrow, T Endo: Determination of the Cyclic Stress-Strain Curve, *J Mater*, 4-1 (1969), 176-188.
- 6) Z Lopez, A Fatemi: A method of predicting cyclic stress strain curve from tensile properties for steels, *Mater Sci Eng A*, 556 (2012), 540-550.
- 7) Z Zhang, Y Qiao, Q Sun, C Li, J Li: Theoretical Estimation to the Cyclic Strength Coefficient and the Cyclic Strain-Hardening Exponent for Metallic Materials: Preliminary Study, *J Mater Eng Perform*, 18 (2009), 245-254.
- 8) G Zonfrillo: New Correlations Between Monotonic and Cyclic Properties of Metallic Materials, *J Mater Eng Perform*, 26 (2017), 1569-1580.
- 9) R Ghajar, N Naserifar, H Sadati, J Alizadeh K: A neural network approach for predicting steel properties characterizing cyclic Ramberg-Osgood equation, 34-7 (2011), 534-544.
- 10) T Marohni, R Basan, M Franulovi: Evaluation of the Possibility of Estimating Cyclic Stress-strain Parameters and Curves from Monotonic Properties of Steels, *Procedia Eng*, 101 (2015), 277-284.
- 11) J Li, Z Zhang, C Li: An improved method for estimation of Ramberg-Osgood curves of steels from monotonic tensile properties, *Fatigue Fract Engng Mater Struct*, 39-4 (2016), 412-426.
- 12) H Nishikawa, Y Furuya: Cyclic Yield Characterization for Low-Carbon Steel with HAZ Microstructures, *Mater Trans*, 60-2 (2019), 207-212.
- 13) P W Bridgman: *Studies in Large Plastic Flow and Fracture*, McGRAW-HILL BOOK COMPANY INC (1952).
- 14) G L Rosa, A Risitano, G Mirone: Postnecking elastoplastic characterization: Degree of approximation in the bridgman method and properties of the flow-stress/true-stress ratio, *Metall Mater Trans A*, 34 (2003), 615-624.
- 15) M Murata, T Nishiwaki, Y Yoshida: Stress Correction Method for Flow Stress Identification by Tensile Test using Notched Round Bar, *J Jpn Soc Technol Plast*, 57-669 (2016), 977-982. (in Japanese)
- 16) J. Polák, M. Hájek: Cyclic stress-strain curve evaluation using incremental step test procedure, *Int J Fatigue*, 13-3 (1991), 216-222.
- 17) K Tanaka, S Nishijima, S Matsuoka, T Abe, et al.: LOW- AND HIGH-CYCLE FATIGUE PROPERTIES OF VARIOUS STEELS SPECIFIED IN JIS FOR MACHINE STRUCTURAL USE, *Fatigue Fract Eng Mater Struct*, 4-1 (1981), 97-108.
- 18) K Hatanaka: Cyclic Stress-Strain Response and Low Cycle Fatigue Life in Metallic Materials, *Jpn Soc Mech Eng Int J Ser A*, 50-453(1984), 831-838. (in Japanese)
- 19) H Furukawa: "Plasticity engineering (I) - Plasticity from the microscopic viewpoint -," *J Jpn Soc Precis Eng*, 38-454 (1972), 976-985. (in Japanese)
- 20) A J K Honeyman: *Sheet Metal Ind*, 34 (1957), 51-65.
- 21) S Takaki: Yielding and Deformation Behavior in Polycrystalline Ferritic Steel, *J Jpn Inst Met Mater*, 83-4 (2019), 107-118. (in Japanese)
- 22) M Etou, S Fukushima, T Sasaki, Y Haraguchi, et al: Super Short Interval Multi-pass Rolling Process for Ultrafine-grained Hot Strip, *ISIJ Int*, 48-8 (2008), 1142-1147.
- 23) D Akama, T Tsuchiyama, S Takaki: Evaluation of Dislocation Density in Cold-Worked Iron as Measured Via X-Ray Diffractometry, *J Soc Mater Sci Jpn*, 66-7 (2017), 522-527. (in Japanese)
- 24) Y Tanaka, S Takaki, T Tsuchiyama, R Uemori: Effect of Grain Size on the Yield Stress of Cold Worked Iron, *ISIJ Int*, 58-10 (2018), 1927-1933.